J. Indian Inst. Sci. 62 (A), Jan. 1980, Pp. 1-36

Cosinusoidally modulated surface wave structures—numerical calculations of characteristics

T. S. RUKMINI AND S. K. CHATTERJEE
Department of Electrical Communication Engineering, Indian Institute of Science, Bangalore 560 012, India

Received on November 29, 1979.

Abstract

Results of computer-aided calculations for the power carried by surface waves, attenuation, surface impedance and the effects of modulation index on the radial field decay, spatial harmonics, etc., are reported. Stability of surface wave modes confirmed by experiment is discussed with the help of stability charts drawn for the modulated structures.

Key words : Modulated surface wave structures, stability of surface wave modes.

1. Introduction

The paper presents a report on the numerical computations of the characteristics for cosinusoidally spatially modulated circular cylindrical metallic corrugated structures excited in E_0 mode based on the theoretical analysis by Chatterjee *et al*[1-3]. It is shown that spatially modulated surface wave structures with low values of modulation index ($\delta < 1$) can support more strongly bound surface waves than uniformly corrugated surface wave structures.

2. Equivalent dielectric constant ε^0

The corrugated region for an uniformly corrugated rod excited in E_0 wave is simulated, as a homogeneous dielectric region of equivalent dielectric constant $\varepsilon^0 = f(s, b, a)$ where s, b and a denote respectively the spacing between any two adjacent discs, radius of discs and radius of the central supporting rod. Since it has been proved[2] that the relative amplitudes (A_m) of Floquet harmonics satisfy the inequality relation $A_m\,(m \neq 0)/A_0\,(m = 0) < 1$, therefore, ε^0 for the fundamental mode ($m = 0$) is calculated by using the relation

$$\varepsilon^0 = \beta_0^2/k_0^2 \tag{1}$$

where, the phase constant β_0 for the fundamental mode is determined from the solution of the following equation[2]

$$\frac{2k_0}{l}\,\frac{J_0(\beta_0 s/2)\sin(\beta_0 s/2)}{\beta_0\gamma_0}\,\frac{K_1(\gamma_0 b)}{K_0(\gamma_0 b)} = \frac{F_1(k_0 b)}{F_0(k_0 b)} \tag{2}$$

where $\beta_0^2 = \gamma_0^2 + k_0^2$ (2.1)

and $l = s + t; \quad t < s$ (2.2)

t = thickness of discs

$$F_1(k_0\rho) = [J_0(k_0 a)\, Y_1(k_0\rho) - Y_0(k_0 a)\, J_1(k_0\rho)]$$

$$F_0(k_0\rho) = [J_0(k_0 a)\, Y_0(k_0\rho) - Y_0(k_0 a)\, J_0(k_0\rho)] \qquad \rho = b \tag{2.3}$$

Figure 1 shows that

(i) the allowed values of ε^0 can be defined for only certain combinations of s and b, for a particular value of k_0, the value of a being held constant ($a = 0{\cdot}25$ cm).

(ii) ε^0 is a decreasing function of s for a fixed value of groove depth ($b - a$).

(iii) For a groove depth $\simeq n\lambda_0/2$, ε^0 approaches the value of unity which is the value for the external medium (air). This implies that a modified 'Harms-Goubau' line approaches 'Sommerfeld' surface wave line when the groove depth for a spatially modulated line approaches the value of integral multiple ($n = 1,2,3\ldots$) of half wavelength ($\lambda_0/2$).

(iv) It is evident that increase of ε^0 is associated with increase of β_0. Therefore, a structure with higher values of ε^0 can support more strongly bound surface wave which is in conformity with the case of Harms–Goubau line.

(v) ε^0 increases with k_0, *i.e.*, with increasing frequency of excitation for allowed values of b and s. Hence, for a surface wave structure with a modified surface, more strongly bound surface wave can be supported with increasing frequency. This is also in conformity with the conventional H–G line.

Hence, it may be concluded that the evolution of the equivalent dielectric concept for the corrugated region for the purpose of analysis is justified.

3. Modulation of ε^0

Since $\varepsilon^0 = f(s, b)$ with the parameter a held constant, spatial or depth modulation is achieved by varying s or b respectively and keeping the other parameter constant. In this case, spatial cosinusoidal modulation is studied.

$$\varepsilon(z) = \varepsilon^0\left(1 - \delta\cos\frac{2\pi z}{L}\right) \tag{3}$$

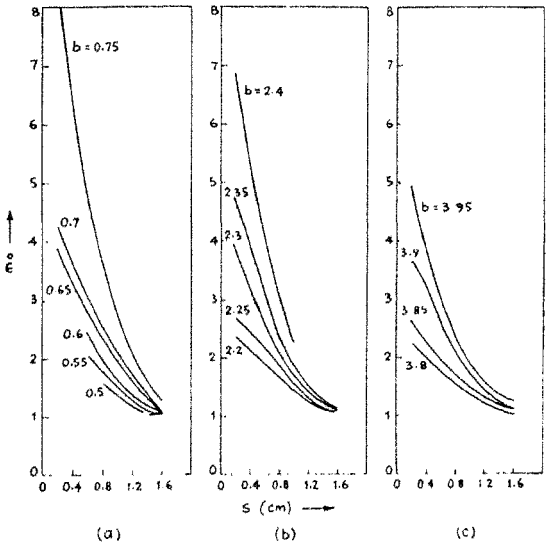

FIG. 1 (*a–c*). Variation of ϵ^0 with spacing(s) with b as parameter.

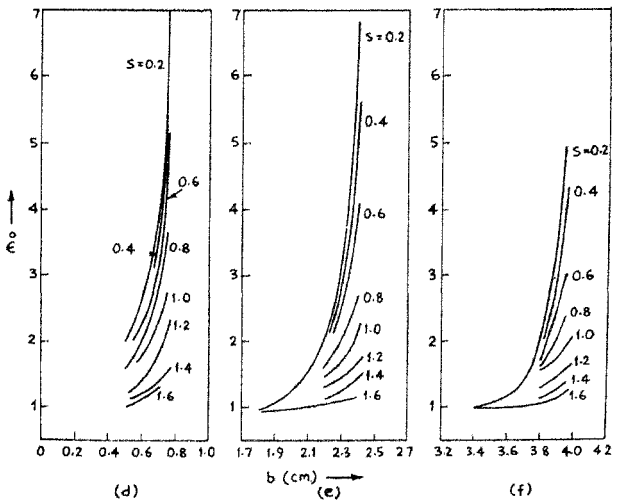

FIG. 1 (*d–f*). ϵ^0 vs b with S as parameter.

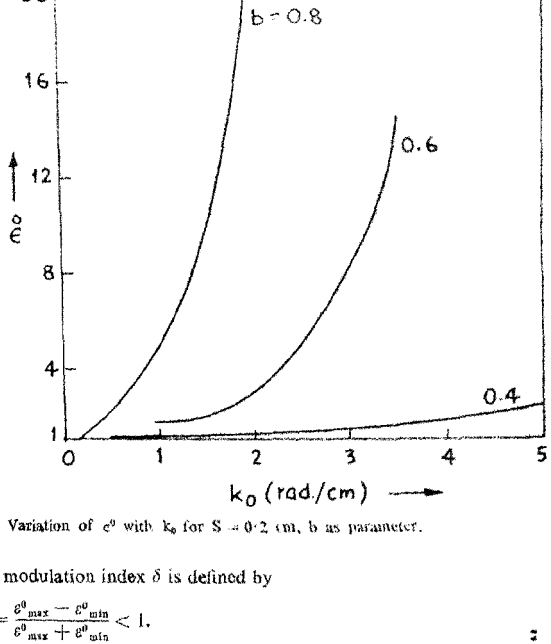

FIG. 1 *g*. Variation of ϵ^0 with k_0 for S = 0·2 cm, b as parameter.

where the modulation index δ is defined by

$$\delta = \frac{\epsilon^0_{max} - \epsilon^0_{min}}{\epsilon^0_{max} + \epsilon^0_{min}} < 1, \tag{3.1}$$

The spacing s is varied over a cell of length L in the direction (z) of propagation. The design of the structures depends on the profile (s-profile or b profile) equations[2]. The variations of s and hence $\epsilon(z)$ over half a period are shown in Fig. 2 which are based on the assumptions $k_0 a < 1$, $k_0 b > 1$, $\gamma_0 b < 1$ and $k_0 a < 1$, $k_0 b < 1$, $\gamma_0 b < 1$ respectively.

4. Radial propagation constants

Using the following mixed boundary condition[3]

$$= \frac{\left[E_{z2} - \frac{(\partial E_{z2}/\partial\rho)^2}{(\partial^2 E_{z2}/\partial\rho^2)}\right]_{\rho=b}}{\left[E_{z1} - \frac{(\partial E_{z1}/\partial\rho)^2}{(\partial^2 E_{z1}/\partial\rho^2)}\right]_{\rho=b}} = \frac{\left[H_{\phi 2} - \frac{(\partial H_{\phi 2}/\partial\rho)^2}{(\partial^2 H_{\phi 2}/\partial\rho^2)}\right]_{\rho=b}}{\left[H_{\phi 1} - \frac{(\partial H_{\phi 1}/\partial\rho)^2}{(\partial^2 H_{\phi 1}/\partial\rho^2)}\right]_{\rho=b}} \tag{4}$$

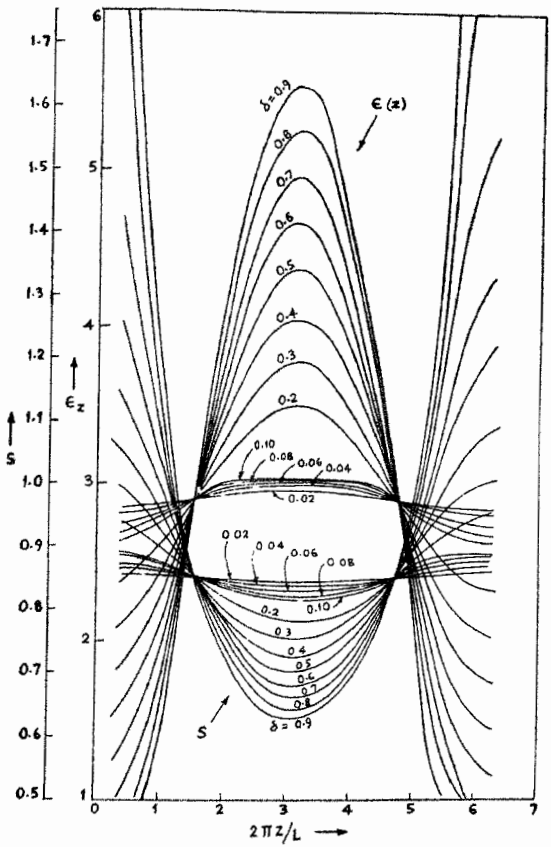

FIG. 2 *a*. Spacing vs $2\pi z/L$ and ϵ_z vs $2\pi z/L$ for case 3. $\epsilon^0 = 2{\cdot}914$, b = 0·3 cm, S = 2·05 cm, a = 0·2 cm.

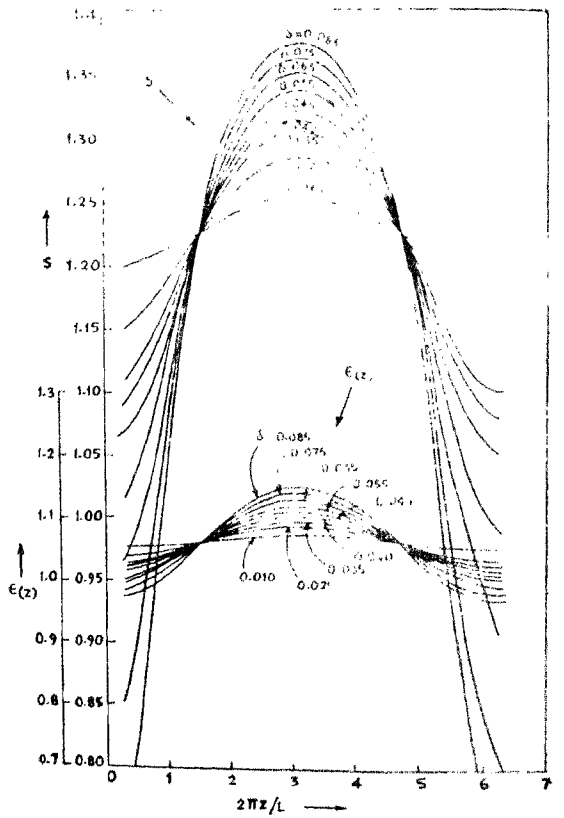

FIG. 2 *b*. ϵ_a and spacing vs $2\pi z/L$ for case 4. ϵ^{b} = 1·062, b = 0·6 cm, S = 1·5 cm, a = 0·25 cm.

and appropriate field components for the two media the following characteristic equation[3] is obtained

$$\left[K_1(k_1b) - \frac{\left\{\frac{K_1(k_1b)}{b} + K_0(k\,b)\right\}^2}{\left\{\frac{2K_1(k_1b)}{b^2} + \frac{K_0(k_1b)}{b} + K_1(k_1b)\right\}}\right] \Bigg/ \left[K_0(k_1b) - \frac{K_1^2(k_1b)}{\frac{K_1(k_1b)}{b} + K_0(k_1b)}\right]$$

$$= \left[\left\{I_1(k_2b) + \frac{I_0(k_2a)}{k_0(k_2a)} K_1(k_2b)\right\} + \frac{\left\{\frac{I_1(k_2b)}{b} \cdot I_0(k_2b) + \frac{I_0(k_2a)}{K_0(k_2a)}\left(\frac{K_1(k_1b)}{b} + K_0(k_2b)\right)\right\}^2}{\left\{\frac{I_0(k_2b)}{b} - I_1(k_2b) - \frac{I_0(k_2a)}{K_0(k_2a)}\left(\frac{2k_1(k_2b)}{b^2} + K_1(k_2b) + \frac{K_0(k_2b)}{b}\right)\right\}}\right]$$

$$\Bigg/ \left[-\frac{I_0(k_2a)}{K_0(k_2a)} K_0(k_2b) + I_0(k_2b) + \frac{\left\{I_1(k_2b) + \frac{I_0(k_2a)}{K_0(k_2a)} K_1(k_2b)\right\}^2}{\left\{\frac{I_1(k_2b)}{b} - I_0(k_2b) + \frac{I_0(k_2a)}{K_0(k_2a)}\left(\frac{K_1(k_2b)}{b} - K_0(k_2b)\right)\right\}}\right] \tag{5}$$

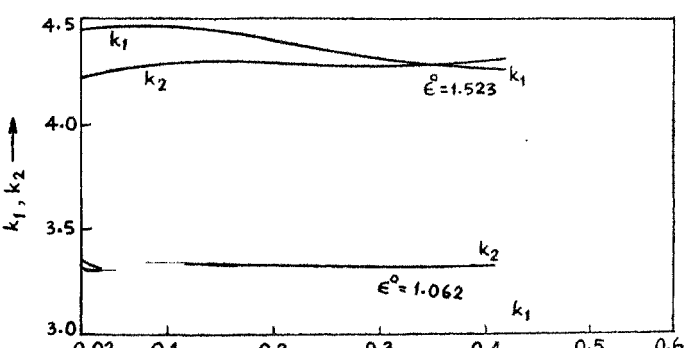

FIG. 3 *a*. Variation of k_1 and k_2 with δ at $z = 0$ with ϵ^0 as parameter.

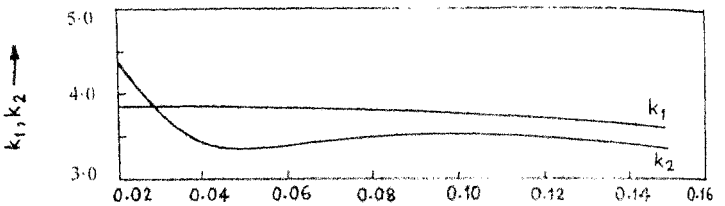

FIG. 3 *b*. Variation of k_1, k_2 with δ at $z = 0$ for $\epsilon^0 = 1{\cdot}293$.

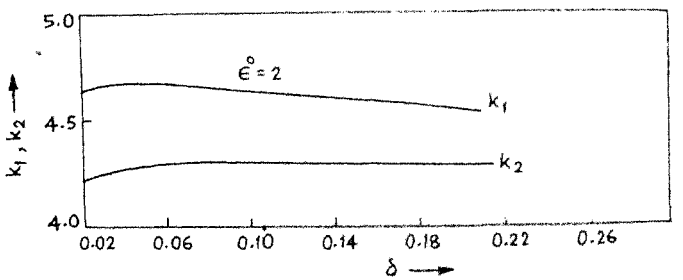

FIG. 3 *c*. Variation of k_1, k_2 with δ at $z = 0$ for $\epsilon^0 = 2{\cdot}0$.

The solution of (5) with

$$k_2^2 = k_1^2 + k_0^2[1 - \epsilon(z)] \tag{6}$$

yields the values of k_1 and k_2 as $f(\delta)$ for fixed values of ϵ^0 (Fig. 3), at $z = 0$. Figure 4 shows the variation of k_1 and k_2 at different locations of the structure over a half period. Figure 5 shows a comparison between k_{1p} and k_{2p} (p: order of modes) between two successive higher order modes.

The following observations may be made regarding k_1 and k_2:

(i) $k_1 > k_2$ for the structure with $\epsilon^0 = 2{\cdot}0$ over the whole range of δ but for structures with $\epsilon^0 = 1{\cdot}062$, $1{\cdot}293$ and $1{\cdot}523$, $k_1 > k_2$ over only a limited range of δ.

(ii) k_2 and $\epsilon(z)$ and hence β are slowly varying functions of $2\pi z/L$, *i.e.*, the locations along the cell length L.

(iii) The different nature of variation of k_1 and k_2 with $2\pi z/L$ for the two modes signifies that the two modes behave differently with regard to radial field decay at different locations of the structures.

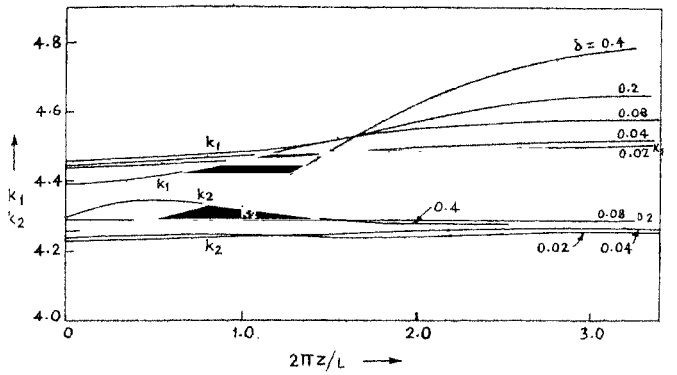

FIG. 4 *a*. Variation of k_1, k_2 with δ for $\epsilon^0 = 1{\cdot}523$ over the period $2\pi z/L$.

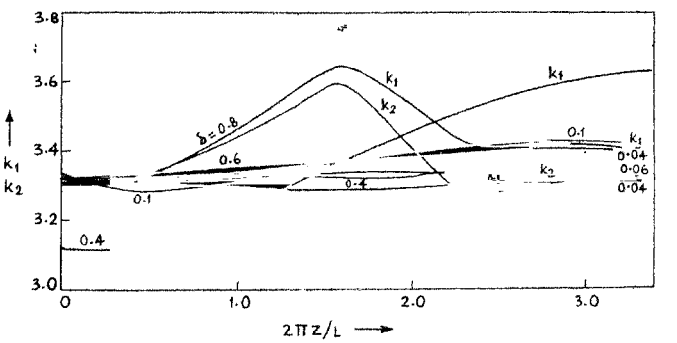

FIG. 4 *b*. Variation of k_1, k_2 with δ for $\epsilon^0 = 1{\cdot}062$ over the period $2\pi z/L$.

(iv) The constants k_{1p}, k_{2p} and β_p in the two media for p modes are related as follows:

$$\beta_p^2 = k_{1p}^2 + k_0^2 \quad (7)$$ First medium (med. 1)

and

$$\beta_p^2 = k_{2p}^2 + k_0^2\,\epsilon(z) \quad (8)$$ Second (modulated) medium (med. 2).

The equalities $k_{11} = k_{12}$, $k_{21} = k_{22}$ at $z = 2{\cdot}35\ L/2\pi$ signify that the two modes become indistinguishable ($\beta_1 = \beta_2$).

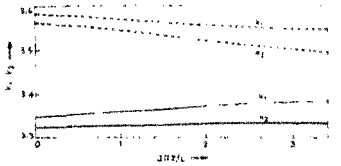

FIG. 5 (a). k_1, k_2 vs $2\pi z/L$ for $\epsilon^0 = 1{\cdot}062$, $\delta = 0{\cdot}02$. — 1st root, - - - 2nd root.

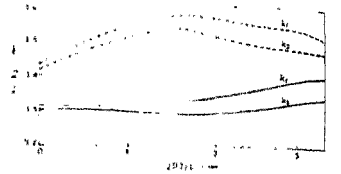

FIG. 5 (b). k_1, k_2 vs $2\pi z/L$ for $\epsilon^0 = 1{\cdot}062$, $\delta = 0{\cdot}04$. — 1st root, - - - 2nd root.

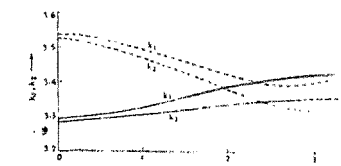

FIG. 5 (c). k_1, k_2 vs $2\pi z/L$ for $\epsilon^0 = 1{\cdot}062$, $\delta = 0{\cdot}05$. — 1st root, - - - 2nd root.

FIG. 5 (d). k_1, k_2 vs $2\pi z/L$ for $\epsilon^0 = 1{\cdot}062$, $\delta = 0{\cdot}06$. — 1st root, - - - 2nd root.

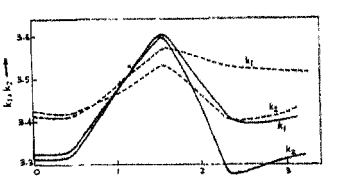

FIG. 5 (e). k_1, k_2 vs $2\pi z/L$ for $\epsilon^0 = 1{\cdot}062$, $\delta = 0{\cdot}08$. — 1st root, - - - 2nd root.

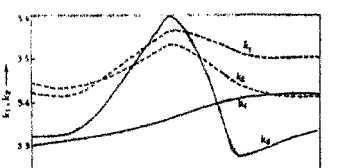

FIG. 5 (f). k_1, k_2 vs $2\pi z/L$ for $\epsilon^0 = 1{\cdot}062$, $\delta = 0{\cdot}1$. — 1st root, - - - 2nd root.

(v) The equality $k_{11} = k_{22}$ signifies that

$$\beta_2^2 - \beta_1^2 = k_0^2 [\epsilon(z) - 1] \tag{9}$$

which means that $\beta_2 > \beta_1$ since $\epsilon(z) > 1$, or in other words, $v_{p2} < v_{p1}$. Hence, the higher order mode is more strongly bound and consequently its rate of radial decay is faster than that of the first mode.

(vi) The equality $k_{12} = k_{21} = k_{22}$ signifies not only the indistinguishability of the two modes in medium 1 but also that $v_{p2} < v_{p1}$.

(vii) The phenomenon of mode crossing observed in some cases is possibly due to coupling of modes arising due to spatial modulation of corrugations.

5. Phase constant (β)

The problem of the propagation of E_0 wave in spatially modulated surface wave structures is formulated in the form of Hill's equation, the solution of which yields the following relation[1]

$$\beta = \frac{2}{\pi} \text{ arc } \sin \left\{ \mathcal{D}[0] \sin^{\pi} \frac{\sqrt{\theta_0}}{2} \right\} \tag{10}$$

where the determinant

$$\mathcal{D}[0] = \frac{\sin^2 \frac{\pi\beta}{2}}{\sin^2 \frac{\pi\sqrt{\theta_0}}{2}} \tag{10 a}$$

and involves θ_n ($n = 0,1,2, \ldots$) where

$$\theta_0 = \left(\frac{k_0 L}{\pi}\right)^2 \left[\epsilon^0 + \left(\frac{k}{k_0}\right)^2 \right] - \frac{3\delta^2}{2} \left(1 + \frac{\delta^2}{4}\right)$$

$$\theta_1 = -\frac{\epsilon^0 \delta}{2} \left(\frac{k_0 L}{\pi}\right)^2 + \left(\delta + \frac{\delta^3}{2} - \frac{3}{4}\delta^5\right)$$

$$\theta_2 = \frac{5}{4}\delta^2 + \frac{\delta^4}{2}$$

$$\theta_3 = \delta^3 + \frac{3\delta^5}{4}$$

$$\theta_4 = \frac{11}{16}\delta^4 + \frac{3}{4}\delta^5, \text{ etc.} \tag{10 b}$$

Where the length of a cell $L = f(\delta, \epsilon^0)$ which can be determined from Fig. 2. The variation of θ_n (up to $n = 4$) with respect to δ is shown in Fig. 6. The variation of $\mathcal{D}[0]$ with δ is shown in Fig. 7.

6. Radial field distributions

The field components in the two media are given by[3]

Med 1: $\quad b \leqslant \rho < \infty$

$$H_{\phi 1} = -i\chi_1 \frac{2A_1}{\pi} K_1(k_1\rho)$$

$$E_{\rho 1} = -i\chi_1 \frac{2A_1}{\pi(\omega\epsilon_0)} K_0(k_1\rho)$$

$$E_{z1} = \chi_2 \frac{2A_1}{\pi(\omega\epsilon_0)} K_1(k_1\rho) \tag{11 a}$$

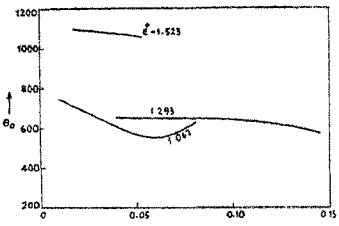

FIG. 6 (*a*). Variation of θ_0 with δ, with ϵ^0 as parameter.

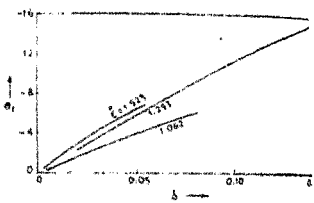

FIG. 6 (*b*). Variation of θ_1 with δ, with ϵ^0 parameter.

Med 2: $a \leqslant \rho \leqslant b$

$$H_{\phi 2} = -A_2 \chi \left[I_1(k_2\rho) + \frac{I_0(k_2 a)}{K_0(k_2 a)} K_1(k_2\rho) \right]$$

$$E_{z2} = -\frac{A_2 \chi}{\omega \epsilon_0 \epsilon(z)} \left[I_0(k_2\rho) - \frac{I_0(k_2 a)}{K_0(k_2 a)} K_0(k_2\rho) \right]$$

$$E_{\rho 2} = -A_2 \chi' \left[I_1(k_2\rho) + \frac{I_0(k_2 a)}{K_0(k_2 a)} K_1(k_2\rho) \right] \qquad (11\,b$$

Where χ and χ^1 involve the Fourier gap coefficients $c_n(\beta)$.

The field distributions (E_z and H_ϕ with ρ) in both the media are shown in Figs. 8 and 9. The following conclusions are of interest.

(i) The radial field decay in the outside medium for modulated ($\delta > 0$) structures is faster than for an uniform ($\delta = 0$) structure. Hence the surface wave is more tightly bound in the case of modulated structures with low modulation index compared to the case of an uniform structure.

(ii) The end-fire property of surface wave modulated structures depends not only on a proper choice of δ but also of L. The fact that better end-fire property can be attained by slow rate of variation of s, *i.e.*, $\epsilon(z)$ is also supported by Billström[4].

(iii) The higher modes decay faster in med. 1 than the lower order modes, since $k_{13} > k_{12} > k_{11}$. The greater concentration of energy towards the interface lead to greater Joulean heat loss for higher order modes than the first order mode. Consequently, the first order mode will be guided to a longer distance along the structure. Hence for a finite length modulated structure, the end-fire radiation will consist mainly of the first order mode.

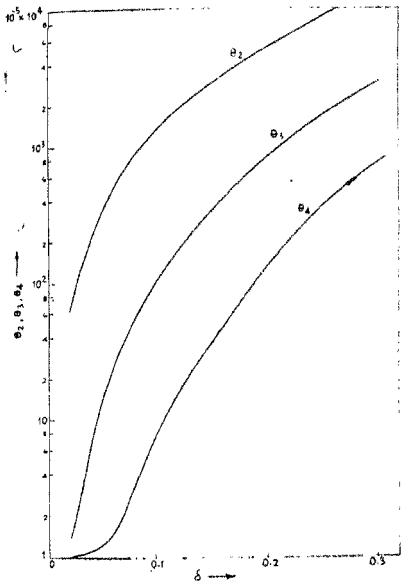

FIG. 6 (c). Variation of θ_2, θ_3, θ_4 with δ.

7. Fourier gap coefficients

The Fourier gap coefficients c_n for uniformly corrugated rod is given by[3]

$$C_n(\beta) = \frac{F_0(k_0\rho)}{F_0(k_0 b)} \frac{\sin \beta_n s/2}{\beta_n s/2} \tag{12}$$

where $\beta_n = \beta_0 + \frac{2\pi n}{l}$

where l is the length of a period and $n = 0, \pm 1, \pm 2, \pm 3$ order of forward (+) and backward (−) space harmonics. $F_0(k_0\rho)/F_0(k_0 b)$ takes into account the nature of the field variation in the radial direction. For a particular value of $c_n = f(\beta_n s/2)$. It is found that over the region $\beta_n s/2 = 0$ to $0{\cdot}4$ c_n is a very slowly varying function of s. Hence, in the case of the spatially modulated structure, the variation of c_n may be considered to be inappreciably small. Hence, $c_n(\beta)$ for the modulated structure may be considered to be the same as c_n in the case of uniform structure without introducing any appreciable error, provided δ is small.

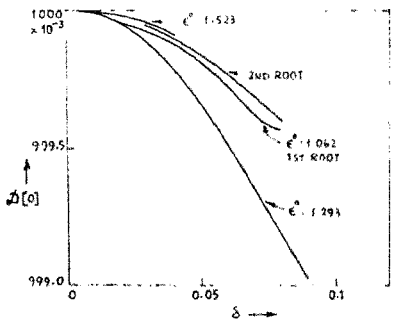

FIG. 7. Variation of $\Phi(0)$ with δ.

The histograms of $C_{\pm n/c_0}$ are shown in Fig. 10. It is observed that

(i) for structures with $\epsilon^0 = 1{\cdot}531$, $1{\cdot}408$ and $1{\cdot}179$, $c_{\pm n}$ $(n \neq 0)/c_0 > 1$ whereas, for structures with $\epsilon^0 = 1{\cdot}062$, $1{\cdot}293$, $1{\cdot}523$ and $1{\cdot}144$ $c_{\pm n} < c_0$.

(ii) All $c_{\pm n}$ $(n \neq 0)$ in the case of structures with $\epsilon^0 = 1{\cdot}531$, $1{\cdot}408$ and $1{\cdot}179$ are less than $c_{\pm n}$ $(n \neq 0)$ for structures with $\epsilon^0 = 1{\cdot}062$, $1{\cdot}293$, $1{\cdot}523$ and $1{\cdot}144$.

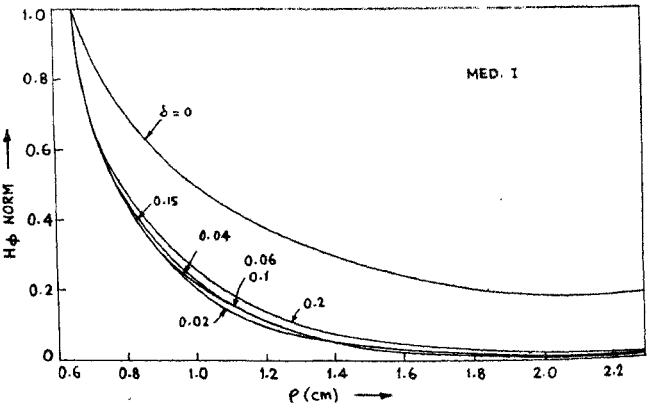

FIG. 8 (*a*). $H\phi$ vs ρ for $\epsilon^0 = 1{\cdot}293$ in medium I.

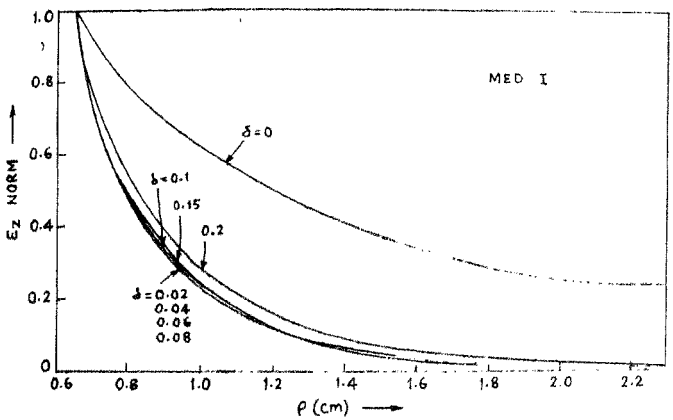

Fig. 8 (b). E_z vs ρ for $\epsilon^0 = 1{\cdot}293$ in medium I.

8. Power flow in modulated structures

The power flow outside (P_z^0) and inside (P_z^1) the modulated medium in the z-direction are given by the following relations[3]

$$P_z^0 = + \frac{4A_1^2}{\pi\omega\epsilon_0} \frac{b^2}{2} \left[\frac{K_0^2(k_1 b)}{K_1^2} + \frac{2}{k_1 b} K_1(k_1 b) K_0(k_1 b) \quad K_1^2(k_1 b) \right] F_n(\beta) \tag{13}$$

$$P_z^1 = - \frac{4A_1^2}{\pi\omega\epsilon_0 \epsilon(z)} \left[\frac{K_0^2(k_1 b) K_1^2(k_2 b)}{\{I_0(k_2 b) K_0(k_2 a) - I_0(k_2 a) K_0(k_2 b)\}^2} \right]$$

$$\left[\frac{1}{2} a^2 \left\{ \frac{I_0^2(k_2 a)}{a^2} - I_1^2(k_2 a) - \frac{2 I_0(k_2 a) I_1(k_2 a)}{k_2 a^2} \right\} \right.$$

$$- \frac{1}{2} b^2 \left\{ \frac{I_0^2(k_2 b)}{b^2} - I_1^2(k_2 b) - \frac{2 I_0(k_2 b) I_1(k_2 b)}{k_2 b^2} \right\}$$

$$+ \frac{I_0^2(k_2 a)}{K_0^2(k_2 a)} \left\{ \frac{1}{2} b^2 \left(\frac{K_0^2(k_2 b)}{b^2} - K_1^2(k_2 b) + \frac{2 K_1(k_2 b) K_0(k_2 b)}{k_2 b^2} \right) \right.$$

$$\left. - \frac{1}{2} a^2 \left\{ \frac{K_0^2(k_2 a)}{a^2} - K_1^2(k_2 a) + \frac{2 K_1(k_2 a) K_0(k_2 a)}{k_2 a^2} \right\} \right\}$$

$$\left. + \frac{I_0(k_2 a)}{K_0(k_2 a)} \frac{(b - a)}{k_2} \right] f_n(\beta) \tag{14}$$

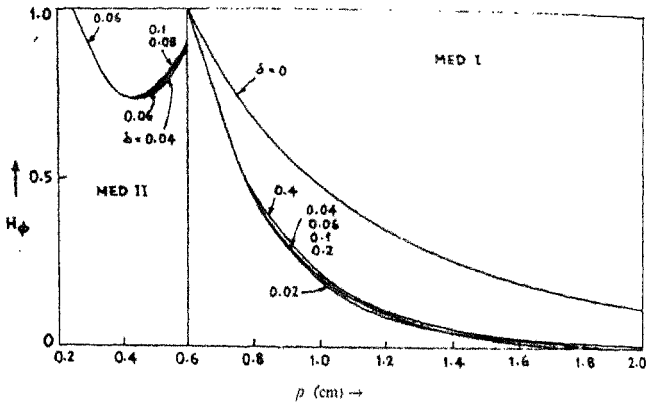

FIG. 8 (c). H_ϕ vs ρ for $\epsilon^0 = 1{\cdot}062$.

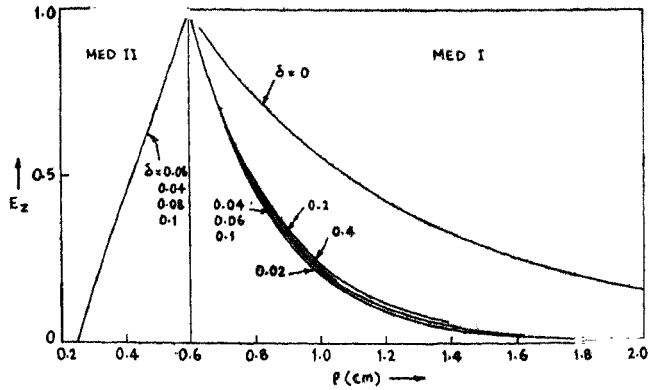

FIG. 8 (d). E_z vs ρ for $\epsilon^0 = 1{\cdot}062$.

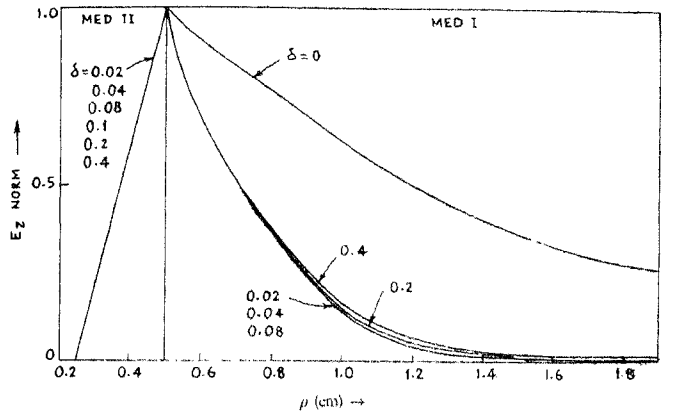

FIG. 8 (*e*). E_z vs ρ for ϵ^0 = 1·523 for different δ_s in media I and II.

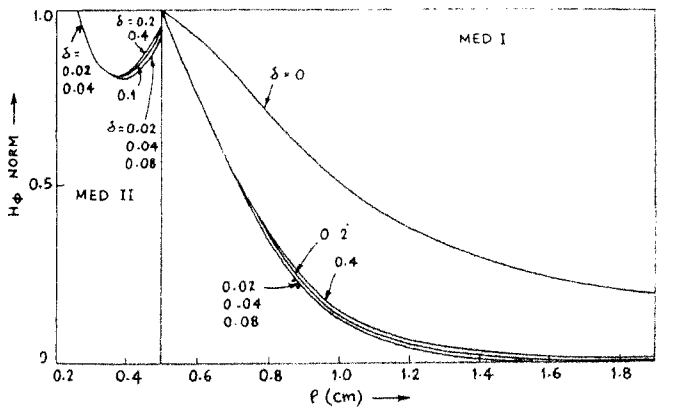

FIG. 8 (*f*). H_ϕ vs ρ for ϵ^0 = 1·523 for different δ_s in media I and II.

where,

$$F_n(\beta) = -\sum_{n=-\infty}^{\infty} c_n(\beta)\cos\theta \sum_{n=-\infty}^{\infty}\left\{\sin\theta\,\frac{d}{dz}c_n(\beta) \pm \frac{\pi}{L}\cos\theta\left(2n+\beta+z\frac{d\beta}{dz}\right)c_n(\beta)\right\}$$

$$\pm\sum_{n=-\infty}^{\infty} c_n(\beta)\sin\theta \sum_{n=-\infty}^{\infty}\left\{\frac{d}{dz}c_n(\beta)\cos\theta \mp \frac{\pi}{L}\sin\theta\cdot\left(2n+\beta+z\frac{d\beta}{dz}\right)c_n(\beta)\right\} \quad (13\,a)$$

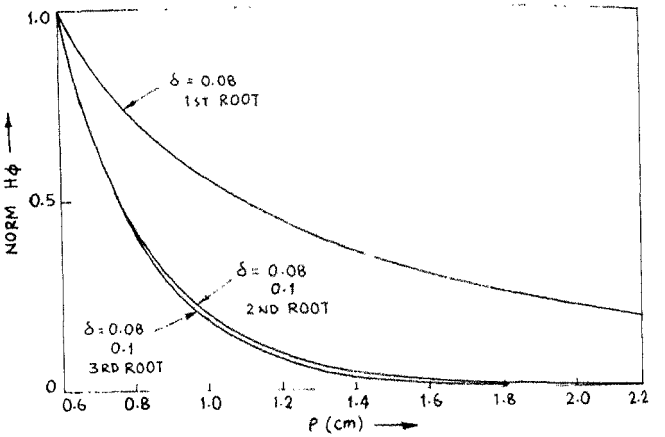

FIG. 9 (*a*). H_ϕ vs ρ for $\epsilon^0 = 1{\cdot}062$.

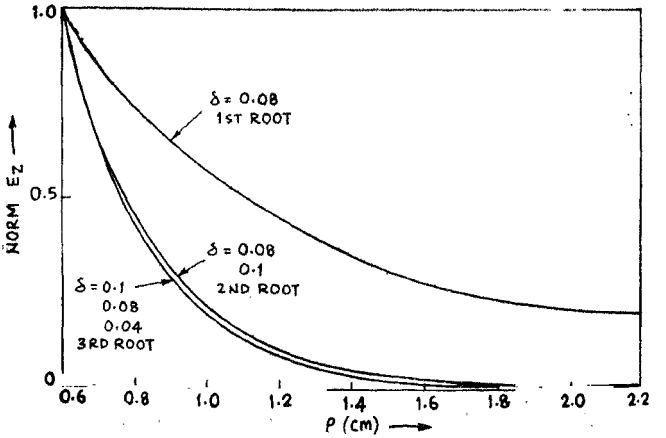

FIG. 9 (*b*). E_z vs ρ for $\epsilon^0 = 1{\cdot}062$.

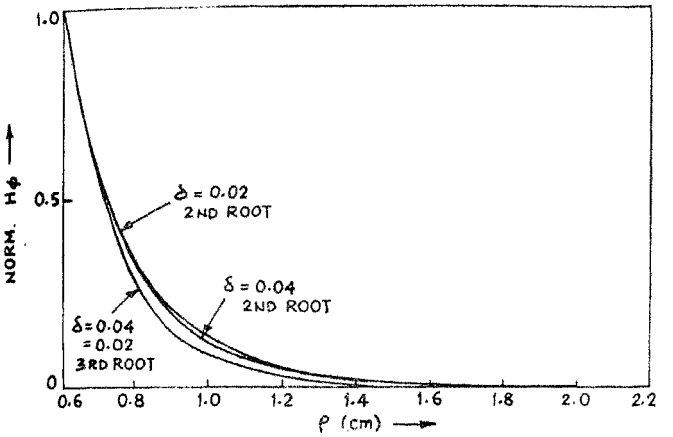

FIG. 9 (c). H_ϕ vs ρ for $\epsilon^{\prime\prime}$ = 1·523.

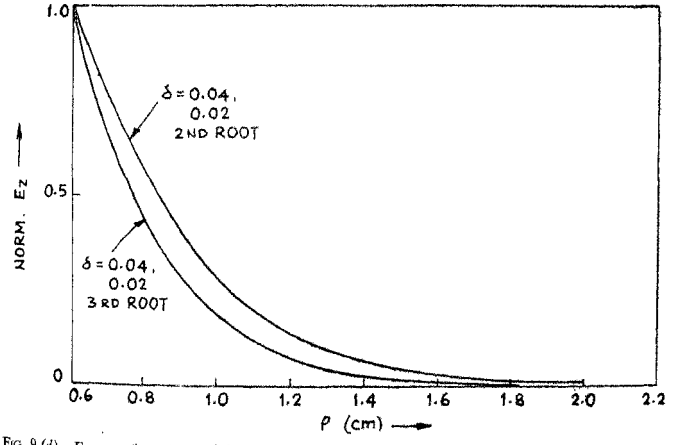

FIG. 9 (d). E_z vs ρ for $\epsilon^{\prime\prime}$ = 1·523.

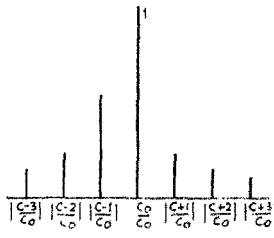

(a) S=0.8cm, b=0.5cm, β_0=2.45, ϵ^0=1.531

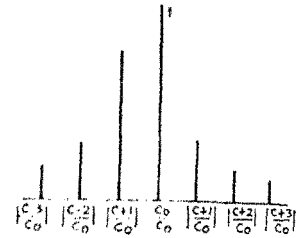

(b) S=1.2cm, b=0.5cm, β_0=2.15, ϵ^0=1.179

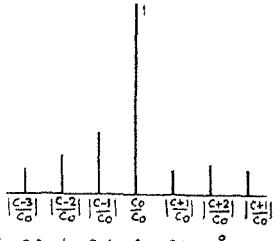

(c) S=0.2, b=0.4, β_0=2.35, ϵ^0=1.408

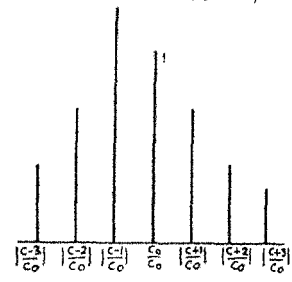

(d) S=1.5, b=0.6, β_0=2.25, ϵ^0=1.062

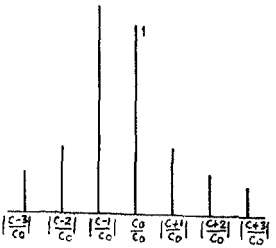

(e) S=1.5cm, b=0.5cm, β_0=2.13, ϵ^0=1.523

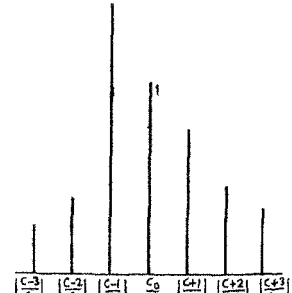

(f) S=1.6cm, b=0.65cm, β_0=2.15, ϵ^0=1.293

FIG. 10. Histograms of gap coefficient c_n/c_0, $n = 0, \pm1, \pm2, \pm3$.

and

$$f_n(\beta) = \left[\mp \frac{2\pi\delta}{L} \sin\frac{2\pi z}{L} \sum_{n=-\infty}^{\infty} c_n(\beta)\cos\theta \sum_{n=-\infty}^{\infty} c_n(\beta)\sin\theta \right]$$

$$\mp\left(1 - \delta\cos\frac{2\pi z}{L}\right)\left(z\frac{d\beta}{dz} + \beta\right)\frac{\pi}{L}\left[\sum_{n}^{\infty} c_n(\beta)\cos\theta \sum_{n=-\infty}^{\infty} c_n(\beta)\cos\theta\right.$$

$$\left. - \sum_{n=-\infty}^{\infty} c_n(\beta)\sin\theta \sum_{n=-\infty}^{\infty} c_n(\beta)\sin\theta \right] \mp \left(1 - \delta\cos\frac{2\pi z}{L}\right).$$

$$\left[\sum_{n=-\infty}^{n} c_n(\beta)\cos\theta \sum_{n=-\infty}^{\infty} \frac{dc_n(\beta)}{dz}\sin\theta + \sum_{n=-\infty}^{\infty} c_n(\beta)\sin\theta \sum_{n=-\infty}^{\infty} \frac{dc_n(\beta)}{dz}\cos\theta\right]$$

$$\mp\left(1 - \delta\cos\frac{2\pi z}{L}\right)\left[\sum_{n=-\infty}^{\infty} c_n(\beta)\frac{2n\pi}{L}\cos\theta \sum_{n=-\infty}^{\infty} c_n(\beta)\cos\theta\right.$$

$$\left. - \sum_{n=-\infty}^{\infty} c_n(\beta)\frac{2n\pi}{L}\sin\theta \sum_{n=-\infty}^{\infty} c_n(\beta)\sin\theta\right] \qquad (14\,a)$$

Where $\theta = \frac{2n\pi z}{L} + \frac{\pi\beta z}{L}$ (14 *b*)

Since β_n is a slowly varying function of z, it does not vary significantly over a period L. Hence, $c_n(\beta)$ does not vary significantly over a period L. The order of smallness of variation may be estimated as (WKBJ approximation).

$$\frac{dc_n}{d\beta} \sim \frac{c_n}{L}, \quad \frac{d^2c_n}{d\beta^2} = \frac{c_n}{L^2} \text{ where } \frac{d^2c_n}{d\beta^2} \ll \frac{dc_n}{d\beta}$$

and hence $\frac{dc_n}{d\beta}$ can be replaced by $\frac{c_n}{L}$ which is equivalent to replacing $\frac{dc_n}{dz}$ by $\frac{c_n}{L}$.

The relative intensities of spatial harmonics $f_{\pm n}\,(n \neq 0)/f_0$ for structures with different values of ϵ^0 and δ shown in Fig. 11 in the form of histograms lead to the following conclusions.

(i) $f_{\pm n}\,(n \neq 0)/f_0 < 1$ for all structures.

(ii) For all structures with any value of δ $f_{-1} > f_{+1}$, but $f_{+n}\,(n > 1) > f_{-n}\,(n > 1)$ for the corresponding values of n.

(iii) For a structure with a particular value of ϵ^0, δ has very little influence on $f_{\pm n}\,(n \neq 0)/f_0$ within the range of $\delta = 0{\cdot}02$ to $\delta = 0{\cdot}1$.

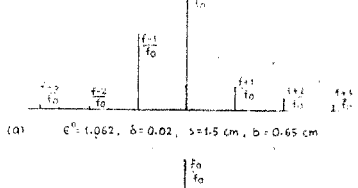

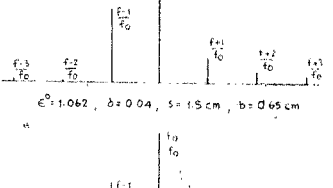

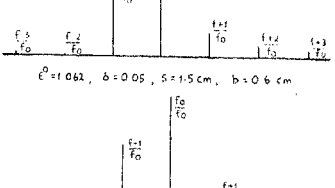

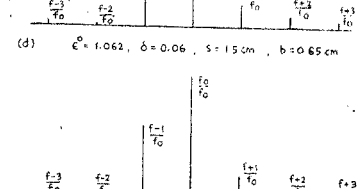

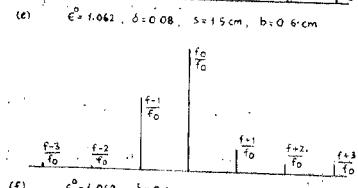

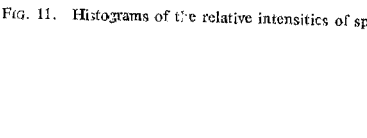

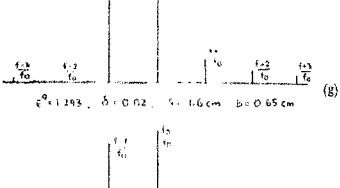

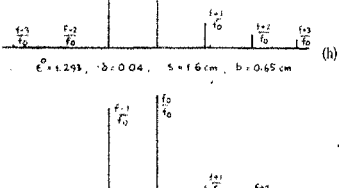

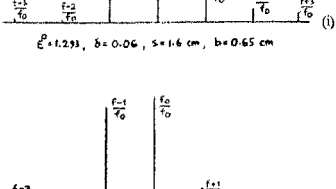

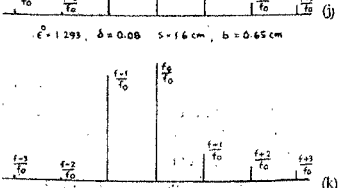

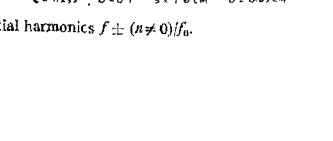

FIG. 11. Histograms of the relative intensities of spatial harmonics $f \pm (n \neq 0)/f_0$.

(iv) $f_{-1} > f_{-n}$ $(n \neq 0,\ n \neq -1)$ for all the structures within the range of $\delta = 0 \cdot 1$.

(v) $\dfrac{f_{-n}}{f_0}\ (n > 1) \leqslant \dfrac{f_{-n}}{f_0}\ (n > 0$ and $n \neq -1)$.

The variation of the ratio of $P_z^n / P_z^T{}_0^n$ with respect to δ and $2\pi z/L$ where $P_z^T = P_z^0 + P_z^1$ presented in Fig. 12 show that

(i) $P_z^0/Pz^T = f(\delta)$ and also depends on the allowed values of β, *i.e.*, the stability of modes.

(ii) P_z^0/P_z^T tends to increase as $\delta \to 0$. In other words the consequence of modulating the structure is to constrain more power to flow in the modulated medium, thus ensuring a more tightly bound surface wave.

(iii) $(P_z^0/P_z^T)_1$ for the first mode associated with the first root of $k_1 b$ and $k_2 b$ is slightly less than $(P_z^0/P_z^T)_2$ for the second mode associated with the second root of $k_1 b$ and $k_2 b$ at different locations in a cell. This is probably due to the functional nature of the roots.

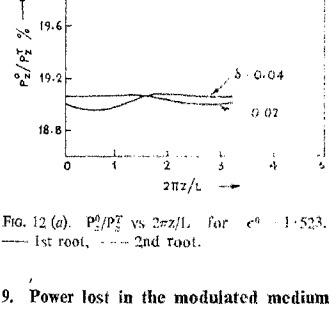

FIG. 12 (*a*). P_z^0/P_z^T vs $2\pi z/L$ for $\epsilon^0 = 1 \cdot 523$. —— 1st root, - - - 2nd root.

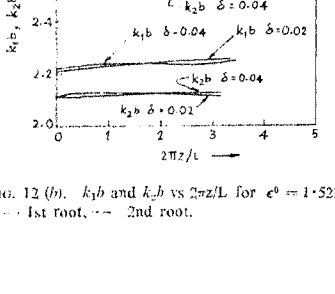

FIG. 12 (*b*). $k_1 b$ and $k_2 b$ vs $2\pi z/L$ for $\epsilon^0 = 1 \cdot 523$. —— 1st root, - - - 2nd root.

9. Power lost in the modulated medium

The power lost in the second (modulated medium) is given by[3]

$$P_L = -\frac{376 \cdot 7}{2} \sqrt{\frac{1}{\epsilon(z)}} \cdot \frac{4A_1^2}{\pi^2} \chi\chi^* \epsilon^0 \epsilon(z) K^2 \left[K_0^2(k_2 a) \left\{ -\tfrac{1}{2} b^2 \left(\frac{I_0^2(k_2 b)}{b^2} - \frac{2I_0(k_2 b) I_1(k_2 b)}{k_2 b^2} - I_1^2(k_2 b) \right) + \tfrac{1}{2} a^2 \left(\frac{I_0^2(k_2 a)}{a^2} - \frac{2I_0(k_2 a) I_1(k_2 a)}{k_2 a^2} - I_1^2(k_2 a) \right) \right\} \right.$$

$$+ I_0^2(k_2a)\left\{\tfrac{1}{2}b^2\left(\frac{K_0^2(k_2b)}{b^2} + \frac{2K_0(k_2b)K_1(k_2b)}{k_2b^2} - K_1^2(k_2b)\right)\right.$$

$$\left. - \tfrac{1}{2}a^2\left(\frac{K_0^2(k_2a)}{a^2} + \frac{2K_0(k_2a)K_1(k_2a)}{k_2a^2} - K_1^2(k_2a)\right)\right\}$$

$$\left. + I_0(k_2a)K_0(k_2a)\frac{(b-a)}{k_2}\right] \qquad (15)$$

where

$$\chi\chi^* = \left(1 - \delta\cos\frac{2\pi z}{L}\right)\sum_{n=-\infty}^{\infty} c_n(\beta)\exp(\pm in\theta)\sum_{n=-\infty}^{\infty} c_n(\beta)\exp(\pm in\theta). \qquad (15\,a)$$

Hence $P_L = f(\delta, \epsilon^0, b, a)$ and β which is involved in θ.

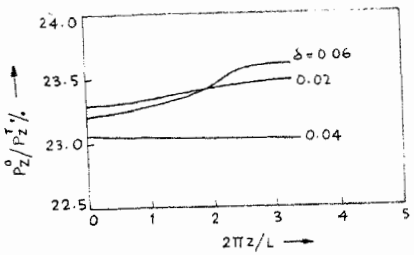

FIG. 12 (c). P_z^0/P_z^T vs $2\pi z/L$ for $\epsilon^0 = 1{\cdot}062$ (1st root).

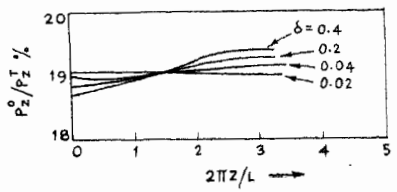

FIG. 12 (d). P_z^0/P_z^T vs $2\pi z/L$ for ϵ^0 1·523 with δ as parameter (1st root).

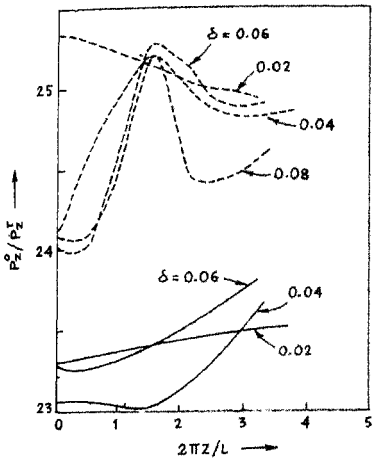

FIG. 12 (e). P_z^0/P_z^T vs $2\pi z/L$ for 1st and 2nd roots for one cell. $\epsilon^\circ = 1{\cdot}062$ with δ as parameter. ——— 1st root, ...2nd root.

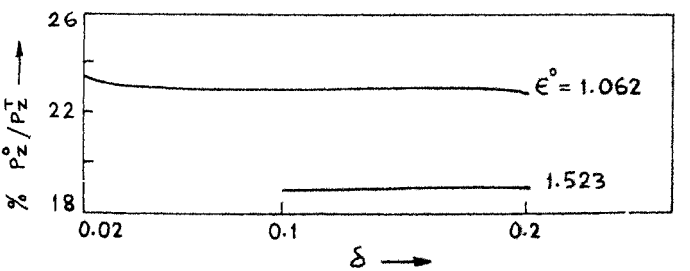

FIG. 12 (f). P_z^0/P_z^T vs δ with ϵ° as parameter (1st root).

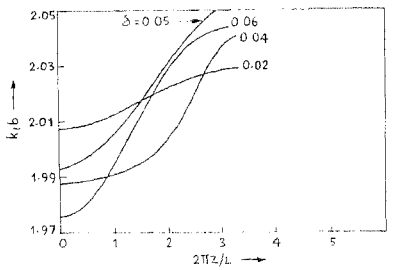

FIG. 12 (*g*). $k_1 b$ vs $2\pi z/L$ for $\epsilon^0 = 1{\cdot}062$ (1st root).

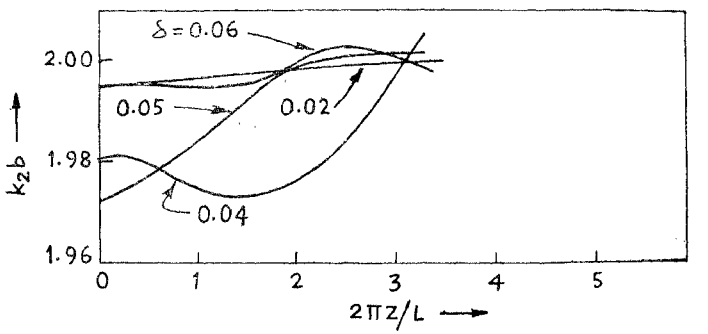

FIG. 12 (*h*). $k_2 b$ vs $2\pi z/L$ for $\epsilon^0 = 1{\cdot}062$ (1st root).

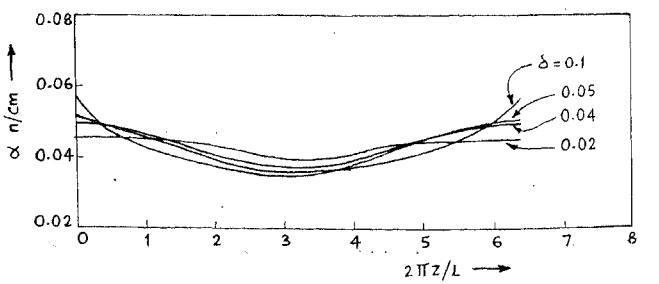

FIG. 13 (*a*). α vs $2\pi z/L$ for different δs for $\epsilon^0 = 1{\cdot}062$.

10. Attenuation constant

The attenuation constant (α) calculated by the power lost method for the fundamental ($n = 0$) component of the wave is given by[3]

$$\alpha\,(\text{nepers/m}) = \frac{\left[188\,\omega\epsilon_0\sqrt{\epsilon^0}\,(1-\delta)\left\{\dfrac{K_0(k_1b)}{I_0(k_2b)\,K_0(k_2a) - I_0(k_2a)\,K_0(k_2b)}\right\}^2 \left\{K_0^2(k_2a)\,.\,f(k_2a, k_2b) + I_0^2(k_2a)\,.\,g(k_2a, k_2b) + I_0(k_2a)\,K_0(k_2a)\,\dfrac{(b-a)}{k_2}\right\}\right]}{\left[\dfrac{1}{2}\,b^2\left\{\dfrac{K_0^2(k_1b)}{K_1^2} + \dfrac{2}{k_1^2b}\,K_1(k_1b)\,K_0(k_1b) - K_1^2(k_1b)\right\} + \dfrac{K_1^2(k_1b)}{\left\{I_1(k_2b) + \dfrac{I_0(k_2a)}{K_0(k_2a)}\,K_1(k_2b)\right\}^2} \times \left\{f(k_2a, k_2b) + \dfrac{I_0^2(k_2a)}{K_0^2(k_2a)}\,.\,g(k_2a, k_2b) + \dfrac{(b-a)}{k_2}\,\dfrac{I_0(k_2a)}{K_0(k_2a)}\right\} 4\beta\cos 2\pi\beta\right]} \tag{16}$$

where

$$f(k_2a, k_2b) = \left[\frac{1}{2}\,a^2\left\{\frac{I_0^2(k_2a)}{a^2} - \frac{2I_0(k_2a)\,I_1(k_2a)}{k_2a^2} - I_1^2(k_2a)\right\} - \frac{1}{2}\,b^2\left\{\frac{I_0^2(k_2b)}{b^2} - \frac{2I_0(k_2b)\,I_1(k_2b)}{k_2b^2} - I_1^2(k_2b)\right\}\right] \tag{16 a}$$

and

$$g(k_2a, k_2b) = \left[\frac{1}{2}\,b^2\left\{\frac{K_0^2(k_2b)}{b^2} + \frac{2K_0(k_2b)\,K_1(k_2b)}{k_2b^2} - K_1^2(k_2b)\right\} - \frac{1}{2}\,a^2\left\{\frac{K_0^2(k_2a)}{a^2} + \frac{2K_0(k_2a)\,K_1(k_2a)}{k_2a^2} - K_1^2(k_2a)\right\}\right] \tag{16 b}$$

(i) As $\delta \to 0$, *i.e.*, $\epsilon^0_{max} \to \epsilon^0_{min}$ *i.e.*, the modulated structure tends towards a uniform structure, α is determined with the understanding that the transverse propagation constants k_1 and k_2 and the axial propagation constant β have the values corresponding to the values of a structure with uniform spacing but with the same values of b and a.

(ii) As $b \to a$ but $(b - a) \neq 0$, *i.e.*, for small depth of corrugation, the terms involving $(b - a)/k_2$ in (16) can be neglected and hence α reduces to

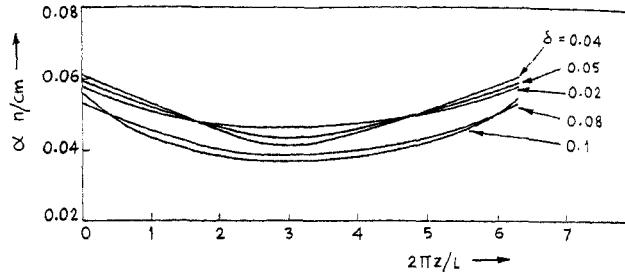

FIG. 13 (*b*). α vs $2\pi z/L$ for different δs for $\epsilon^0 = 1{\cdot}523$.

$$188\,\omega\epsilon_0\sqrt{\epsilon^0(1-\delta)}\left\{\frac{K_0(k_1b)}{I_0(k_2b)\,K_0(k_2a) - I_0(k_2a)\,K_0(k_2b)}\right\}^2$$

$$\alpha\ (\text{nepers/m})\ (b \to a)\ (b - a \neq 0) = \frac{\{K_0^2(k_2a)\,f(k_2a, k_2b) + I_0^2(k_2a)\,g(k_2a, k_2b)\}}{\left[\frac{1}{2}b^2\left\{\frac{K_0^2(k_1b)}{k_1^2} + \frac{2}{k_1^2b}K_1(k_1b)\,K_0(k_1b) - K_1^2(k_1b)\right\}\right.}$$

$$\left. + \frac{K_1^2(k_1b)}{\left\{I_1(k_1b) + \frac{I_0(k_2a)\,K_1(k_2b)}{K_0(k_2a)}\right\}^2} \times \left\{f(k_2a, k_2b) + \frac{I_0^2(k_2a)}{K_0^2(k_2a)}g(k_2a, k_2b)\right\}\right] \tag{17}$$

(i) The variation of α *vs* $2\pi z/L$ (Fig. 13) shows that $\alpha_{max} - \alpha_{min}$ is much less for lower values of $\delta = 0{\cdot}02$, $0{\cdot}04$ than for higher values of δ.

(ii) α_{min} for all values of δ is attained at $2\pi z/L = \pi$.

(iii) $\alpha_{av}\,(\delta \neq 0)$ (Table I) calculated by considering values of α at 1/16th interval over one period is greater than $\alpha\,(\delta = 0)$.

(iv) $\alpha_{av}\,(\delta \neq 0) > \alpha\,(\delta = 0)$ is justified since

$$\frac{P_z^0}{P_z^T}\%\,(\delta = 0) > \frac{P_z^0}{P_z^T}\%\,(\delta > 0).$$

The outside medium, being air, is lossless. Hence the loss for the guided wave is contributed by only the physical properties of the modulated medium.

(v) For shallow grooved structures α *vs* $2\pi z/L$ (Fig. 14) shows that (Table II) $\alpha_{av} \sim a$ is higher compared to that given in Table I.

Table I

a_{av} **(nepers cm)**

$\epsilon' = 1{\cdot}062$ [$\alpha(\delta = 0) = 0{\cdot}001$ nepers/cm)]					
δ	·02	·04	·06	·08	0·1
a_{av}	0·0582	0·0565	0·0501	0·0496	0·0481
$a_{av} - \alpha$	0·0572	0·0555	0·0491	0·0486	0·04707
$\epsilon' = 1{\cdot}523$ [$\alpha(\delta = 0) = 0{\cdot}002$ nepers/cm]					
a_{av}	0·0494	0·0481	0·0476	0·04758	0·04757
	0·0474	0·0461	0·0456	0·04558	0·04557

Table II

$a_{av} - a$ **for shallow grooved structures**

$\epsilon' = 1{\cdot}062$					
δ	0·02	0·04	0·06	0·08	0·1
$a_{av} - \alpha$	0·5512	0·5424	0·5396	0·5308	0·5292
$\epsilon' = 1{\cdot}523$					
$a_{av} - \alpha$	0·7931	0·7927	0·7915	0·7901	0·7891

Since the corrugated line approaches Sommerfeld line as $b \to a$, *ohmic dissipation giving* rise to Joule heat loss is mainly responsible (radiation loss being neglected in both the cases) for supporting surface waves, it is reasonable to expect that

$$\alpha\,(\text{shallow grooved line}) > \alpha\,(b > a)$$

$$b \to a$$

11. Surface impedance

The real and imaginary parts of surface impedance are given in the following dimensionless form[3]

$$\frac{2\pi b}{\lambda_0}\frac{R_s}{Z_0} = \frac{1}{\epsilon(z)}\left[a_1 b \ln 0{\cdot}89\,(a_1^2 b^2 + b_1^2 b^2)^{1/2} - b_1 b \arctan\frac{b_1 b}{a_1 b}\right] \qquad (18\,a)$$

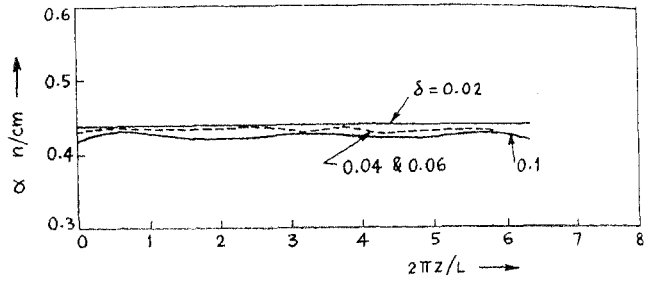

FIG. 14 (*a*). α vs $2\pi z/L$ for different δs for $\epsilon^0 = 1{\cdot}062$.

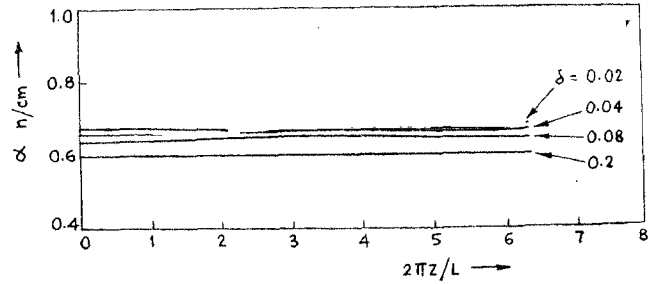

FIG. 14 (*b*). α vs $2\pi z/L$ for different δs for $\epsilon^0 = 1{\cdot}523$.

and

$$\frac{2\pi b}{\lambda_0}\frac{X_s}{Z_0} = -\left[a_1 b \arctan\frac{b_1 b}{a_1 b} + b_1 b \ln 0{\cdot}89\,(a_1^2 b^2 + b_1^2 b^2)^{1/2}\right] \tag{18b}$$

where $k_1 = a_1 - ib_1$ and $b_1 = \dfrac{\alpha\beta}{a_1}$

$$a_1 = [\tfrac{1}{2}\{(\beta^2 - \alpha^2 - k_0^2) \pm \sqrt{(\alpha^2 - \beta^2 + k_0^2)^2 + 4\alpha^2\beta^2}\}]^{1/2}. \tag{19}$$

The radial field decay and attenuation depend respectively on X_s and R_s which are influenced by δ. Figure 15 provides design data for developing a structure characterised by a rapid radial field decay and with minimum attenuation. It is desirable to have high positive surface reactance (inductive) and low surface resistance. $X_s = I_m(Z_s)$ $R_s = \mathrm{Re}\,(Z_s)$ are $f(\delta, \epsilon^0)$ and location (z) along the structure, hence the average values are plotted in Fig. 15. The average values have been calculated by considering the values of the parameters at 1/16 interval over a whole period.

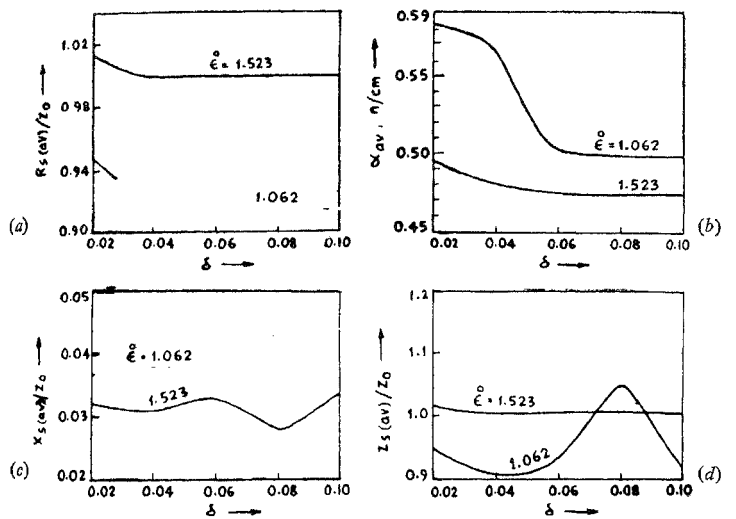

FIG. 15 (*a–d*) (*a*) $R_{s(av)}/Z_0$ vs δ for $\epsilon^0 = 1{\cdot}062$ and $\epsilon^0 = 1{\cdot}523$. (*b*) α_{av} n/cm vs δ for $\epsilon^0 = 1{\cdot}523$ and $\epsilon^0 = 1{\cdot}062$; (*c*) $X_{s(av)}/Z_0$ vs δ for $\epsilon^0 = 1{\cdot}062$ and $\epsilon^0 = 1{\cdot}523$; (*d*) $Z_{s(av)}/Z_0$ vs δ for $\epsilon^0 = 1{\cdot}062$.

We conclude from Fig. 15 that

(i) For structure with $\epsilon^0 = 1{\cdot}062$, the design should be for $\delta = 0{\cdot}08$ or $0{\cdot}1$ so that high rate of radial field decay with low attenuation can be obtained.

(ii) For structure with $\epsilon^0 = 1{\cdot}062$, the design should be for $\delta = 0{\cdot}06$ or $0{\cdot}1$.

12. Measurement of radial field decay

Radial field decay for several modulated and a uniform corrugated structures was measured with a monopole probe (Fig. 16) and the results are compared with theory (Fig. 17). In the second and fourth illustrations of Fig. 17, the experimental (00) and theoretical curve coincide for $\delta = 0$, whereas, for $\delta = 0{\cdot}04$ there is a slight divergence between the two curves.

We conclude, that for modulated structures, the rate of radial field decay is faster than for uniform structure.

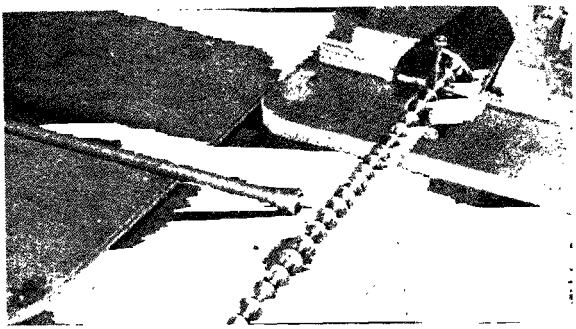

FIG. 16. Photograph of the structure.

13. Stability of the surface wave mode

The stability charts (Fig. 18) for structures with $\epsilon^0 = 1{\cdot}062$ for $\delta = 0{\cdot}08$ and $0{\cdot}25$ have been prepared with β as a parameter by using the equation (10) with the aid of a 360 IBM computer. (The Flow Chart is not reported).

The stable solutions corresponding to modulated propagating waves are associated with the β-values bounded according to the following inequality relation

$$p \leq \beta \leq p + 1 \, (p = 0,1,2,3). \tag{20}$$

The regions (hatched) which do not satisfy (20) correspond to the unstable solutions of (10). The unstable solutions are associated with the non-propagating or damped waves. The values of β are real within the shaded regions (unshaded), whereas they are complex within the unstable regions. As $\beta = f(\epsilon^0, \delta)$ and $\epsilon^0 = f(s, b, a)$ and δ determines the propagating or non-propagating nature of waves, the stability charts which determine k_a can be used for the design of proper modulated structures which support strongly bound surface waves.

The location of the mode supported by the experimental structure $\epsilon^0 = 1{\cdot}062$, $\delta = 0{\cdot}08$ is shown in Fig. 18 (a). The experimental point $\oplus$ lies within the unshaded region $\beta = 3$ and $\beta = 4$, thus indicating that the mode supported by the structure is stable. It is found that the modes supported by other experimental structures with $\epsilon_0 = 1{\cdot}062$ and $\delta = 0{\cdot}06$, $0{\cdot}04$ and $0{\cdot}1$ also lie in the stable regions of stability charts which are not reported.

Figure 18 (b) shows stability diagrams for the structure with $\epsilon^0 = 1{\cdot}062$ and $\delta = 0{\cdot}25$. Similarly, the stability diagrams have also been drawn for other structures with $\delta = 0{\cdot}08$ and $0{\cdot}25$ for which no experimental structures were made.

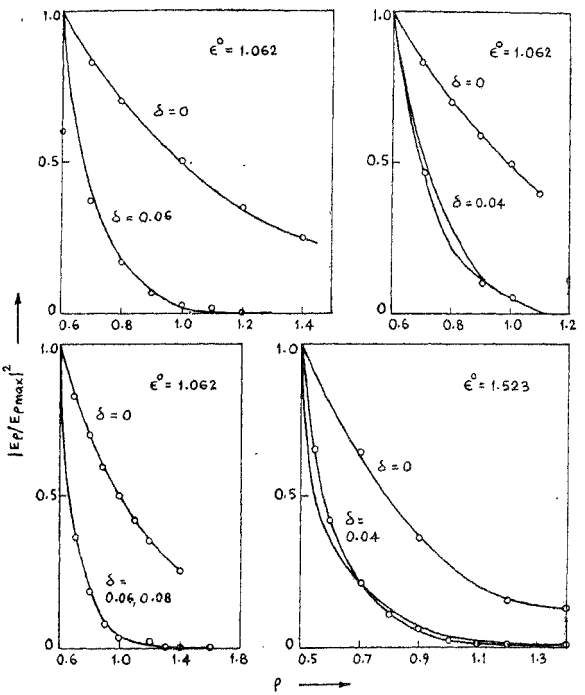

FIG. 17. Variation of power with radial distance. ○ ○ Experimental, —— Theoretical.

The following remarks regarding the stability charts are of interest.

(i) The curves separating the stable and unstable regions in some cases cross over each other, for example, near the points $\theta_0 = 440, 480, 580$, etc. (Fig. 18 (*a*)) where

$$\theta_0 = \left(\frac{k_0 L}{\pi}\right)^2 \left[\epsilon^0 + \left(\frac{k}{k_0}\right)^2\right] - \frac{3}{2}\delta^2\left(1 + \frac{\delta^2}{4}\right)$$

(ii) The area of the stable regions increase as the value for β increases. There is also a tendency for the separation to increase between two adjacent cross-over points as β increases. As a consequence of increase in β, the waves become

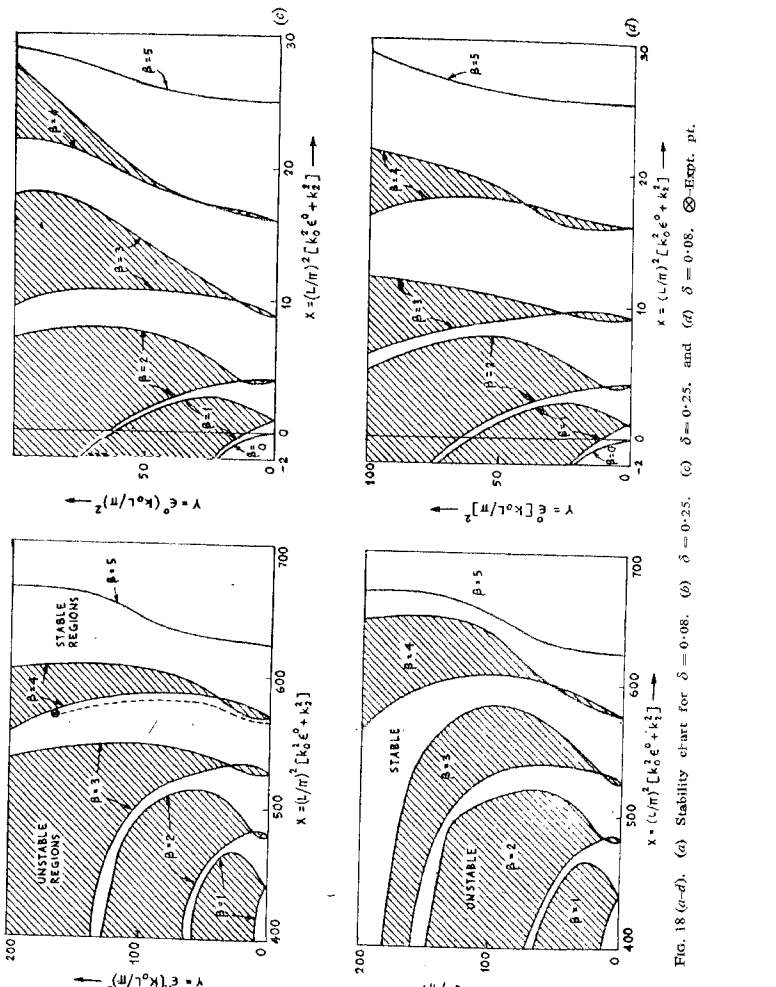

FIG. 18 (*a–d*). (*a*) Stability chart for $\delta = 0{\cdot}08$. (*b*) $\delta = 0{\cdot}25$. (*c*) $\delta = 0{\cdot}25$, and (*d*) $\delta = 0{\cdot}08$. ⊗-Expt. pt.

more strongly bound. Hence, it may be said, that the structure for which the wave is most strongly bound will exhibit the largest area of stable region with widely separated cross-over points in the stability chart. Hence, the usefulness of the stability chart for designing a space modulated structure is obvious.

14. Basic assumptions and their limitations

The theoretical derivation of β for space modulated structures is based on the following assumptions.

(i) The nonuniformly corrugated metallic structure is considered as a conductor coated with a dielectric whose dielectric constant varies cosinusoidally in the direction of propagation.

(ii) $\delta < 1$. This helps in truncating the series for θ_n $(n = 1, 2, \ldots)$ which is involved in $\mathcal{D}[0]$ and hence for β.

(iii) For deriving the profile equation for the design of a practical structure, small and large argument approximations for the Bessel functions have been introduced from practical considerations. This may impose some limitations on the accuracy of the results. But considering the accuracy which can be attained, in practice, in fabricating the structure it is considered that the argument approximations are valid for all practical purposes.

(iv) The simulated dielectric medium is considered lossless in deriving β.

(v) In deriving the magnitudes of the spatial harmonics, βn and hence the Fourier gap coefficients $c_n(\beta)$ is considered to be a slowly varying function over a period of the modulation cycle, which leads to simplification of the expression for $f_n(\beta)$.

(vi) The coating thickness of the equivalent dielectric is considered the same as $(b - a)$.

(vii) In deriving β_0, the field outside the structure is considered to be pure surface wave field and the effect of diffraction is ignored. The assumption, however, is justified in view of the higher value of β_0 and hence a lower value for v_p. This is conferred by the experimental measurement of radial field decay.

15. Conclusions

(i) Cosinusoidal modulation of spacing between discs of circular cylindrical metallic corrugated structures lead to more strongly bound stable surface waves.

(ii) Corrugated metallic structures may be considered as equivalent to a conductor coated with equivalent dielectric whose dielectric constant is a function of the spacing between discs, radius of the discs and radius of the central supporting rod.

(iii) The corrugated modulated region provides inductive reactance which helps in supporting surface waves.

(iv) The attenuation constant decreases with increase in the value of δ.

(v) The power flow outside the modulated structure with respect to the total power flow decreases with increasing δ.

16. Acknowledgement

It is a pleasure to acknowledge the invaluable suggestions by Dr. James R. Wait (ESSA, NOAA), Monitor PL-480 Programme (Contract-E-262-69 (N), 1969) and the financial assistance at the initial stages of the problem by the PL-480 authorities.

Our grateful thanks are also to Prof. (Mrs.) R. Chatterjee, Chairman, Department of Electrical Communication Engineering, for encouragement and helpful discussions.

References

1. CHATTERJEE, S. K., RUKMINI, T. S. AND CHATTERJEE, R. — Propagation of E_0 wave in modulated artificial dielectric media, *J. Indian Inst. Sci.*, 1977, **59** (A), 225–45.

2. CHATTERJEE, S. K. AND RUKMINI, T. S. — Simulation of cosinusoidally modulated dielectric medium by artificial dielectric at microwave frequencies, *J. Indian Inst. Sci.*, 1978, **60** (A), 47–64.

3. CHATTERJEE, S. K., RUKMINI, T. S. AND CHATTERJEE, R. — Surface waves in a nonuniformly corrugated cylindrical metallic structure, *J. Indian Inst. Sci.*, 1978, **60** (A), 119–134.

4. BILLSTRÖM, O. — *E.M. Theory and Antennas*, Edited by E. C. Jordan, Pergamon Press, London, 1963, p. 875.